

## Direct Finite Element Design Optimisation of the Cageless Reluctance Synchronous Machine

M.J. Kamper, F.S. van der Merwe  
Department of Electrical and Electronic Engineering  
University of Stellenbosch, Banhoek Road  
Stellenbosch, 7600, South Africa

S. Williamson, Fellow IEEE  
Department of Engineering  
Cambridge University, Trumpington Street  
Cambridge, CB2 1PZ, United Kingdom

**Abstract**—The finite element analysis method is used directly in optimisation algorithms to optimise in multidimensions the design of the cageless reluctance synchronous machine. Two optimisation methods are evaluated to minimise or maximise the function value. These are the direction set method of Powell and the quasi-Newton algorithm. Both methods proved to be successful, with some advantages and disadvantages. Using these methods at a power level below 10 kW, results are given of structures of the reluctance synchronous machine which have been optimised according specific criteria. Calculated and measured results show that the maximum torque optimum designed reluctance synchronous machine has the advantages of high power density and high efficiency.

### I. INTRODUCTION

The reluctance synchronous machine (RSM) has received attention in the past 5 years as a possible alternative machine for AC drive applications [1, 2]. Hitherto attention was given to the optimum control of the current space phasor of the machine [3, 4] and to the optimum design of the machine, specifically the rotor [5, 6, 7]. Almost no attention, except to some extent for the work of Vagati [5], is given to the optimum design of the stator or to an overall (stator and rotor) optimum design. Further, most of the design analysis is done by means of the lumped circuit model of the RSM. The finite element model is merely used to investigate the effect of the variation of a single dimension on e.g. the inductances of the machine [6, 7] and not to do an overall optimum design.

The question to be answered is what the performance capability or goodness is of the optimum designed RSM. To truly investigate this it is necessary to do an overall design optimisation and to use an analytical model of the machine in the optimisation process which is representative of the real machine. The latter is particularly important for the RSM where the calculation of the q-axis inductance e.g. has to be very accurate and where the effect of cross magnetisation has to be taken into account [7]. The lumped circuit model will

96 WM 145-3 EC A paper recommended and approved by the IEEE Electric Machinery Committee of the IEEE Power Engineering Society for presentation at the 1996 IEEE/PES Winter Meeting, January 21-25, 1996, Baltimore, MD. Manuscript submitted July 27, 1995; made available for printing December 5, 1995.

not give absolute optimisation results. The absolute optimum-designed machine can at best be obtained by using the finite element method in the optimisation process. The purpose of the paper is to show how this can be done and to discuss results of optimised RSM's in the sub 10 kW power range. The type of rotor structure investigated is the cageless, normal laminated rotor with flux barriers. Measured results of an optimised 9 kW RSM in a standard 5.5 kW induction machine frame are given.

### II. FINITE ELEMENT OPTIMISATION

With the power and speed of workstations available today it is possible to use the finite element model of the machine in the optimisation procedure directly. The use of the finite element method in the design optimisation may be explained by the flow diagram of Fig. 1. Here, the optimisation algorithm finds the multidimensional vector  $[X]$ , i.e. the values of the machine variables, that minimises (maximises) the function value  $Y$  or performance parameter of the machine. In this process with each iteration  $r$  the algorithm determines directions of search in a multidimensional space along which  $Y$  is minimised (maximised). Each time the finite element program is called to calculate  $Y$ , a new mesh is generated according to the changed input dimensions  $[X]$ . The program then does the pre-processing and the nonlinear solution to find

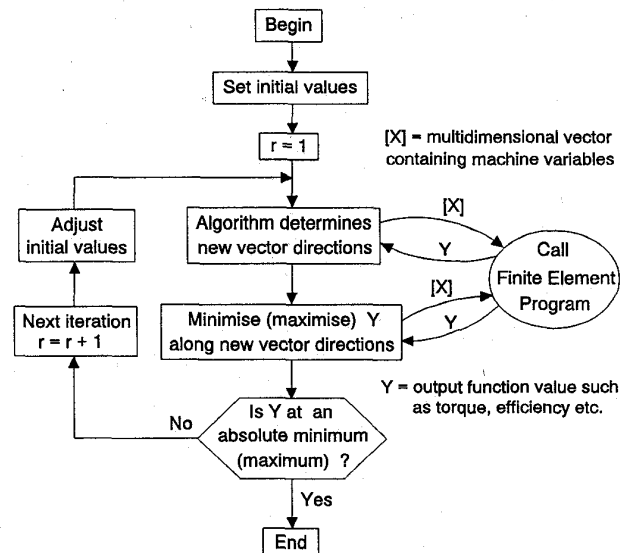


Fig. 1. Optimisation procedure using the finite element solution directly.

the magnetic vector potentials. The flux linkages and flux densities are calculated, followed by the calculation of the output performance parameters (Y) of the machine. The finite element program may be called a number of times by the algorithm during an iteration. At the end of each iteration a test is carried out to determine if an absolute minimum (maximum) is reached. If not, a next iteration is executed.

It is obvious that the process of Fig. 1 will be time consuming which necessitates in the first place that the multidimensional optimisation algorithm be fast. Secondly, it will be beneficial if the performance parameters of the machine can be calculated by using the results of one basic set of finite element solutions. In section III this is shown to be possible for the RSM.

For the optimisation two unconstrained algorithms are used as described in section IV. The focus of the optimisation study is more on the unconstrained condition, although constrained optimisation is also done by using penalty functions.

### III. THE FINITE ELEMENT PROGRAM

This section describes the calculation of the output performance parameters, i.e. the function values like torque, efficiency, power factor, kVA, etc. of the RSM, by means of the finite element program of Fig. 1. The finite element program determines and uses the equivalent circuit parameters of the RSM to calculate the output parameters.

The approximate steady-state d- and q-axis equivalent circuits of the RSM in the rotor reference frame are shown in Fig. 2. The parameters  $R_s$  and  $R_c$  are respectively the per phase winding resistance and per phase core loss resistance, while  $L_e$  is the per phase endwinding leakage inductance. The flux linkages  $\lambda_d$  and  $\lambda_q$  are the d- and q-axis stator flux linkage components, which includes the stator leakage flux linkage but not the endwinding flux linkage. The parameter  $\omega_r$  is the electrical speed of the rotor reference frame. In the phasor diagram the angle  $\theta$  is the power factor angle and  $\phi$  the current space phasor angle. The current phasor  $I_{s1}$  represents the actual current of the machine.

To calculate the equivalent circuit parameters of Fig. 2 the winding resistance  $R_s$  is calculated from the active copper area available at a temperature of, by convention, 75°C. The copper area is determined from the given slot dimensions. The endwinding leakage inductance  $L_e$  is calculated separately using

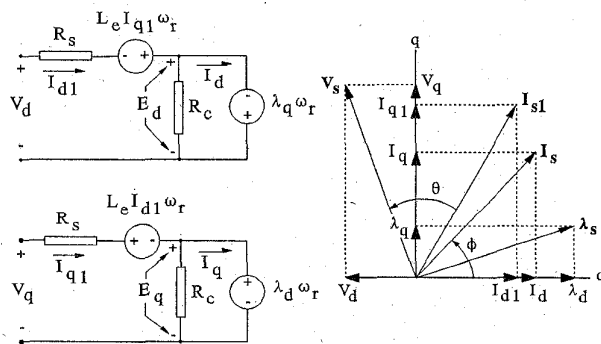


Fig. 2. Steady-state d- and q-axis equivalent circuits and space phasor diagram of the RSM.

a formula derived by Honsinger [8]. This formula is adapted in [9] to correctly take into account the mutual flux linkage between the endwinding phase groups using the computation method of Lawrenson [10].

To calculate the flux linkages using the finite element method it is necessary to specify the phase current  $I_s = \hat{I}_s \angle \phi$  of the machine. Due to the fact that the RSM is under direct current control, the current space phasor can be set at an angle  $\phi$  with respect to the rotor (Fig. 2). The angle  $\phi$  is thus an input variable. The amplitude of the current space phasor,  $\hat{I}_s$ , is determined from either a given rms current density,  $J$ , as given by

$$\hat{I}_s = \sqrt{2} J a_{sc} n_a \quad (1)$$

where  $n_a$  is the number of parallel circuits and  $a_{sc}$  is the active copper area of a stator conductor, or from a given copper loss  $P_{cu}$ , as given by

$$\hat{I}_s = \sqrt{2 P_{cu} / (3 R_s)} = K n_a \sqrt{P_{cu} a_{sc}} \quad (2)$$

Note that the actual current density and copper losses will be slightly higher due to the slightly higher actual winding current  $I_{s1}$  that includes the core loss currents (Fig. 2). With the current space phasor known in terms of amplitude and angle, the  $dq$  current components  $I_{dq}$  can be calculated as well as the instantaneous three-phase currents  $i_{abc}$  using the inverse Park transformation. Hence, the three-phase winding currents are set in the machine according to the rotor position, after which the finite element method is called to calculate the total three-phase flux linkages  $\lambda_{abc}$ . Due allowance is made for saturation by using the correct BH-curve in the finite element program.

The finite element software used is not of the commercial variety. It makes use of triangular elements of the first order. Only one pole (stator and rotor) of the RSM is meshed with one airgap element comprising nodes on both sides of the airgap. A time-saving scheme has been devised [11] that makes the use of one airgap element very attractive as a means to model rotor movement. The Newton-Raphson method is used for the solution of the set of non-linear equations.

The effect of skew is accounted for in the 2-D finite element analysis by using a set of unskewed machines of which the rotors are relatively displaced by an angle that is a fraction of the total skew. The technique is first proposed by [12] and is also used by [13]. With  $k$  submachines the flux linkages are calculated by (3) where  $\lambda_{abc}(\alpha_n)$  denotes the total phase flux linkages of the unskewed machine with the rotor at position  $\alpha_n$ . In this analysis  $k$  is taken as 5.

$$[\lambda_{abc}] = \frac{1}{k} \left[ \sum_{n=1}^k \lambda_{abc}(\alpha_n) \right] \quad (3)$$

Eqn (3) suggests that  $k$  time-expensive finite element field solutions are required, but it is only the first non-linear solution at position  $\alpha_1$  which will take time due to the unknown reluctivities. At positions  $\alpha_2, \dots, \alpha_k$ , the known reluctivities of previous positions can be used, which will already be close to the new reluctivities, so that the field solution times at these positions will be less [12].

The flux linkages of (3) will contain harmonics and it is necessary to obtain the fundamental total flux linkages. With a distributed double layer stator winding it is assumed, as an approximation, that the effects of the MMF space harmonics

are negligible. The remaining harmonic fluxes are the synchronous harmonic fluxes which stand still with respect to the fundamental rotating flux wave. With the rotor skewed no prominent high frequency slot ripple will be present in the flux linkage wave [12, 13]. Further, with a distributed winding the quasi-square flux density wave in the airgap, due to saturation, will be filtered so that a near sinusoidal flux linkage wave is obtained. However, a prominent 3rd and less prominent 5th and 7th harmonics will still be present in the total flux linkage waveform. If the 5th, 7th and higher harmonics are ignored, the total flux linkage can be written in terms of a fundamental and a 3rd harmonic, or

$$[\lambda_{abc}] \approx [\lambda_{abc1}] + [\lambda_{abc3}] \quad (4)$$

The co-phasal 3rd harmonic flux linkages can be obtained, including the higher order co-phasal harmonics, from the actual three-phase flux linkages as

$$\lambda_{a3} = \lambda_{b3} = \lambda_{c3} \approx \frac{1}{3} (\lambda_a + \lambda_b + \lambda_c) \quad (5)$$

Thus, with the actual total phase flux linkages and the 3rd harmonic flux linkages known from the finite element analysis, the fundamental total phase flux linkages can be calculated by (4). With the fundamental total phase flux linkages and the rotor position known, the  $dq$  flux linkages of Fig. 2 are calculated using Park's transformation

$$[\lambda_{dqo}] = [K_s] [\lambda_{abc}] \quad (6)$$

From this the speed voltages of the equivalent circuits of Fig. 2 can be determined. The only remaining parameter to be calculated is the core loss resistance. Considering only stator core losses due to the main flux and fundamental supply frequency of the machine, the iron core losses are

$$P_c = c f_1^x (B_{mt}^y M_t + B_{my}^y M_y) \quad (7)$$

where  $B_{mt}$  and  $B_{my}$  are respectively the maximum flux densities in the teeth and yoke,  $M_t$  and  $M_y$  are respectively the iron masses of the teeth and yoke and  $f_1$  is the fundamental supply frequency. The maximum flux densities in the teeth and yoke can be obtained directly from the finite element solution. The constants  $c$ ,  $x$  and  $y$  are determined from measurements on electrical machines and also from the loss-frequency curves of the laminations used. These constants are taken as  $c=7.5$ ,  $x=1.32$  and  $y=2$  in this analysis. The core loss resistance can be determined as

$$R_c = 3 E_a^2 / P_c \quad (8)$$

where  $E_a$  is the rms value of the phase EMF and is given by

$$E_a = \sqrt{(E_d^2 + E_q^2)} / 2 \quad (9)$$

With all the equivalent circuit parameters known, the  $dq$  currents  $I_{dq1}$  and supply current  $I_{s1}$  are determined, followed by the calculation of the  $dq$  supply voltages and the power factor of the machine. The steady-state torque of the RSM in the rotor reference frame is given by

$$T = \frac{3}{4} p (L_{dm} - L_{qm}) \hat{I}_s^2 \sin(2\phi) \quad (10)$$

where  $L_{dm}$  and  $L_{qm}$  are the d- and q-axis inductances of the RSM due to the d- and q-axis fundamental *airgap* flux linkage components. The latter can be determined from a Fourier

expansion of the radial component of the airgap flux density [7]. In (10),  $p$  is the number of pole pairs. Alternatively the torque can be written

$$T = \frac{3}{4} p (L_d - L_q) \hat{I}_s^2 \sin(2\phi) \quad (11)$$

where  $L_d$  and  $L_q$  are the d- and q-axis inductances due to the d- and q-axis *total* fundamental stator flux linkage components. These inductances are defined as

$$L_d = \lambda_d / I_d \quad \text{and} \quad L_q = \lambda_q / I_q \quad (12)$$

The flux linkages  $\lambda_d$  and  $\lambda_q$  of (12) may be calculated from (4) - (6), but it must be realised that the calculated torque then, using (11) and (12), is subjected to a small error due to the approximation of (4). Finally, the wind and friction losses are taken the same, as an approximation, as that of a same volume standard induction machine. Hence, the shaft torque and efficiency can be calculated.

This concludes the calculation of the performance parameters of the RSM, i.e. the function value  $Y$  of Fig. 1. The effects of cross magnetisation, saturation and skew are taken into account by using the results of just one set of finite element solutions.

#### IV. OPTIMISATION ALGORITHMS

This section focuses on the flow diagram of Fig. 1 where the optimisation algorithm determines new directions of search and minimises (maximises) the function values along these directions. In this process the algorithm repeatedly calls the finite element program to calculate the function values, as described in section III. Two *unconstrained* optimisation algorithms are evaluated namely Powell's method and the finite-difference quasi-Newton algorithm. These methods are briefly described in sections B and C below. Constrained optimisation is done by using the penalty function method as described in section D.

##### A. Line Minimisation

Both optimisation methods considered here make use of successive line minimisations to minimise (maximise) sequentially a function of  $n$  variables along certain lines or vector directions in an  $n$ -dimensional space. For the line minimisation (13) is used, i.e. find the scalar  $y$  that minimises the function  $F(\mathbf{X})$  along a given vector direction  $\mathbf{Z}$  from a given starting vector point  $\mathbf{P}_0$ .

$$\mathbf{X} = \mathbf{P}_0 + y\mathbf{Z} \quad (13)$$

To bracket the minimum (maximum) of the function, the  $y$ -value of (13) is changed in relatively large steps until the minimum (maximum) of the function  $f(y)=F(\mathbf{P}_0+y\mathbf{Z})$  has been bracketed by the values  $y_i$ ,  $y_{i+1}$  and  $y_{i+2}$ . These last three  $y$ -values are then used to do a curve fitting to obtain a second degree interpolating polynomial of the Newton form. The variation of  $f(y)$  with  $y$  gives very smooth curves, as is shown e.g. in the graphs of [7], so that the use of just three points for curve fitting is justified. The minimum (maximum) of the polynomial can be obtained by setting the derivative equal to zero and solving for  $y$ . This solve of  $y$  is then accepted as the location of the minimum of  $F(\mathbf{X})$  along the line (13).

### B. Powell's Method

The method of Powell [14], which is also described in detail by others [16, 17], minimises with each iteration  $r$  the function value along a set of  $n$  vector directions ( $n$  is the number of variables to be optimised). The initial set of  $n$  vector directions are the unit or co-ordinate directions. With each iteration a new direction is defined which is used in the set of vector directions for the next iteration. The basic procedure generates after  $n$  iterations a set of  $n$  mutually conjugate vector directions. This implies that after  $n$  iterations the exact minimum of a quadratic function is found.

Powell modifies the basic procedure because occasionally the procedure may choose nearly dependent directions which may cause the process to terminate before an optimum is reached. Tests are made after each iteration to determine whether the new direction is a good direction to be added to the set of directions or not.

Consider an iteration of Powell's Method where a function is minimised through  $n$  line minimisations which moves the vector point  $\mathbf{P}$  from  $\mathbf{P}_0$  to  $\mathbf{P}_n$  through  $n$  vector directions. If it takes an average of  $m$  finite element program solutions per line minimisation (actually it is  $mk$  program solutions due to skew), then  $mn$  solutions are necessary per iteration. If say  $n$  iterations are used to minimise or maximise the function value, then the total number of finite element solutions will be  $mn^2$  (with  $n=10$  and  $m=3$  the number of solutions are 300). It is thus clear that with a high average number of finite element solutions per line minimisation, the total number of solutions will be high using Powell's Method. The only advantage of Powell's method is that derivatives are not necessary.

### C. Quasi-Newton Algorithm

The quasi-Newton method [15, 16, 17] requires that at each iteration-step,  $r$ , the function's gradient vector  $\mathbf{G}_r$  (vector of first partial derivatives) be calculated at the vector point  $\mathbf{P}_r$ . The new direction of search  $\mathbf{Z}_r$  from this point is given by

$$\mathbf{Z}_r = -\mathbf{H}_r \mathbf{G}_r \quad (14)$$

where  $\mathbf{H}_r$  is an  $n \times n$  matrix which is the quasi-Newton approximation of the inverse Hessian. In the quasi-Newton method the matrix  $\mathbf{H}_r$  is updated sequentially to build up a good approximation of the inverse Hessian. It can be shown that for a quadratic function the algorithm terminates in at most  $n$  steps, where  $n$  is the number of variables to be optimised. The first partial derivative of the function with respect to a variable  $x_i$  is determined by the forward-difference approximation as given by (15).

$$\frac{\partial f}{\partial x_i} \approx \frac{f(x_i + \delta) - f(x_i)}{\delta}; \quad \{\delta = x_i h\} \quad (15)$$

The choice of  $h$  in (15) is critical because it determines the quality of the derivative. If  $h$  is too large then the truncation error is large; if too small then the condition error, due to the error in the computed function value, is large. The usual approximation is to take  $h$  as  $h = \epsilon_r^{1/2}$  where  $\epsilon_r$  is the relative error in the computed function value. Note that function values are not available to machine precision due to the nonlinear finite element field solution which uses an iterative method with a convergence criterium to solve for the magnetic

vector potentials. The accuracy of the computed function value is approximately estimated by using a difference table as described in [15]. Hence,  $h$  was found to be equal to  $10^{-6}$ , but faster optimisation results were obtained with  $h$  between  $10^{-4}$  and  $10^{-5}$ . The error in the finite difference gradient approximation can also be minimised by changing or updating  $h$  as the optimisation progresses [18]. This, however, was found to be unnecessary and a fixed value of  $h=10^{-5}$  was used throughout the optimisation.

By using (15) it is clear that  $n$  finite element program solutions ( $n$  is the number of variables to be optimised) are necessary to determine the gradient vector. With an average of  $m$  solutions to do the line-minimisation and with say  $n$  iteration-steps necessary to minimise the function value, the total number of finite element solutions will be  $n^2 + mn$  (with  $n=10$  and  $m=3$  the number of solutions are 130). This is dramatically less than the  $mn^2$  solutions necessary with Powell's method, particularly when  $m$  is high. However, owing to the inaccuracy of the forward-difference approximation additional iterations will be performed closer to the optimum.

### D. Constrained Optimisation

The penalty function method is used for the constrained optimisation. The objective function is modified by adding terms or functions that assign a positive 'penalty' for increased constraint violation. The new objective function or penalty function is defined as

$$F(\mathbf{X}, \mathbf{w}) = f(\mathbf{X}) + \sum_{i=1}^u w_i c_i(\mathbf{X}) \quad (16)$$

where  $f(\mathbf{X})$  is to be minimised,  $w_i$  are weighting factors and  $c_i(\mathbf{X})$  are functions which penalise infeasibility. As an example, the quadratic penalty function is used to maximise the power factor,  $P_f(\mathbf{X})$ , of the machine subject to the torque constraint  $T(\mathbf{X}) \geq T_0$  as defined by

$$F(\mathbf{X}, \mathbf{w}) = P_f(\mathbf{X}) - w \epsilon \quad (17)$$

where

$$\epsilon = \begin{cases} 0 & : T(\mathbf{X}) \geq T_0 \\ (T_0 - T(\mathbf{X}))^2 & : T(\mathbf{X}) < T_0 \end{cases} \quad (18)$$

The advantage of the penalty function method is that (16) e.g. can now be solved by the use of an unconstrained optimisation algorithm. One disadvantage of this method is that it may require repeated minimisation of  $F(\mathbf{X}, \mathbf{w}_i)$  for a sequence of  $w_i$ .

### E. Results

The Powell and quasi-Newton methods are used to optimise, as an example, five variables of the RSM for two cases where the torque and torque/kVA as function values are maximised (see section V for more detail). The stator variables are the tooth width, yoke height and stator inner diameter, while the rotor variables are two flux barriers widths (see Fig. 3). Due to limited space only the final results of these calculations are given in Table I. As can be seen both methods give the same optimum results for the dimensions which verifies that the optimum dimensions obtained are correct. The relatively high

TABLE I: OPTIMISATION RESULTS OF THE POWELL AND QUASI-NEWTON METHODS

RSM variables (mm) ↓	Max. Torque		Max. Torque/kVA	
	Powell	Q-Newton	Powell	Q-Newton
Tooth width	5.4	5.4	6.3	6.3
Yoke height	18.3	18.3	16.0	15.8
Inner diameter	105.7	105.5	138.9	139.5
Outer barrier	2.9	2.9	3.4	3.4
Inner barrier	5.8	5.9	10.3	10.4
No. of solutions	102	98	156	115

number of finite element program solutions required is due to the strict termination criterium set in the optimisation process. The computation time per finite element program solution is about 5 minutes on a SUN 1000 work-station using an average of 1800 elements per pole and 1100 vector potential unknowns.

In general it was found that the quasi-Newton method is faster than Powell's method. With Powell's method it was found that as the number of variables increases there is a tendency for new directions to be chosen less often (Powell [14] also mentioned this aspect). The weakness of the quasi-Newton algorithm is that additional iterations are performed closer to the optimum due to the approximation of (15).

## V. OPTIMISED RSM STRUCTURES

An overall design optimisation is done of the RSM using the direct finite element optimisation method described in sections II-IV. The optimisation is done for RSM's with the same outer dimensions as that of a standard 5.5 kW induction machine. The rotors of the RSM's are four-barrier per pole rotors with cutouts (Figs. 3 and 4) and are skewed in the analysis by one stator slot pitch. No more than four barriers and cutouts are used to avoid iron losses in the rotor iron segments due to stator slotting [5]. The variables not changed in the optimisation process are: *stator outer diameter* = 203.2 mm, *stack length* = 133.4 mm, *number of stator slots* = 36, *7/9 chorded stator winding*, *airgap length* = 0.34 mm, *web widths* = 1.0 mm and *rib heights* = 0.75 mm. The variables of the RSM to be optimised are (some are shown in Figs. 3 and 4):

$yh$  = stator yoke height;  $tw$  = stator tooth width;  
 $id$  = stator inner diameter;  $iw$  = inner flux barrier width;  
 $ow$  = outer flux barrier width;  
 $ip$  = inner barrier position at rotor surface;  
 $op$  = outer barrier position at rotor surface;  
 $cd$  = cutout dimension;  $ang$  = current angle  $\phi$ ;

These nine variables are optimised by maximising different performance parameters (function values) of the RSM for the given volume. These parameters are maximum torque (T), maximum efficiency ( $\eta$ ), maximum torque per kVA (T/kVA) and constrained maximum torque per kVA. The constrained T/kVA optimisation is done similarly to (17) and (18), subject to a torque constraint of  $T \geq 35$  Nm. In the design optimisation either the copper losses or the current density are kept constant in the finite element program (see (1) and (2)).

The current density is set to  $J=6$  A/mm<sup>2</sup> which is the full-load current density of a standard 5.5 kW induction machine. For the copper losses a  $P_{cu}=700$  W is used which is about the total copper losses of the standard induction machine. Note that the actual current density and copper losses will be slightly higher due to the actual current  $I_{s1}$  of the machine (Fig. 2).

In Table II some of the dimensions of five optimised RSM's are given as well as the performance results. The dimensions and performances of the five machines are discussed in the paragraphs below.

1) *Maximum Torque*: Machines 1 and 2 of Table II are optimised by maximising the output torque. The difference in the stator dimensions ( $yh$ ,  $tw$  and  $id$ ) of these machines can be explained by using the torque equation of the RSM (11) and replacing the current  $I_s$  with either (1), for a given  $J$  (take  $\phi$  as constant)

$$T = K_1 (L_d - L_q) J^2 a_{sc}^2, \quad (19)$$

or (2) for a given  $P_{cu}$

$$T = K_2 (L_d - L_q) P_{cu} a_{sc}. \quad (20)$$

The torque of (19) is proportional to the square of the stator conductor area, or the stator slot area, while the torque of (20) is directly proportional to this area. This explains why the stator dimensions of machine 1 are less than that of machine 2, just to obtain more copper area.

Machine 1 has a very low inductance ratio  $\sigma=L_d/L_q$  (also a

TABLE II: DIMENSIONS AND PERFORMANCES OF DIFFERENT FINITE ELEMENT OPTIMISED RSM'S.

	Machine 1	Machine 2	Machine 3	Machine 4	Machine 5
Criterion	T	T	$\eta$	T/kVA	T/kVA
Constraint →	$J=6$ A/mm <sup>2</sup>	$P_{cu} =$ 700 W	$P_{cu} =$ 700 W	$J=6$ A/mm <sup>2</sup>	$T \geq$ 35 Nm
Variables↓	Optimum values of variables				
yh (mm)	14.96	18.6	18.78	15.57	19.1
tw (mm)	4.39	5.49	5.31	6.2	6.92
id (mm)	96.2	105.1	108.1	140.0	115.8
iw (mm)	6.69	5.76	6.52	10.39	6.92
ow (mm)	2.73	2.87	3.48	3.53	2.88
cd (mm)	3.13	2.89	2.77	13.2	6.32
ang (°)	65.4	63.7	66.3	70.4	61.0
Parameter	Performance results at 1500 r/min				
T (Nm)	57.4	58.1	57.3	22.9	35.0
$\eta$ (%)	88.6	89.6	89.7	88.2	89.6
$P_{out}$ (kW)	9.02	9.13	8.99	3.6	5.5
$P_{cu}$ (W)	818	721	721	314	376
$P_{iron}$ (W)	296	291	260	119	214
$P_{factor}$	0.606	0.682	0.709	0.81	0.745
kVA	16.8	14.94	14.14	5.03	8.24
J (A/mm <sup>2</sup> )	6.07	6.95	7.02	6.13	6.13
$L_d-L_q$ (mH)	30.6	50.0	54.2	103.8	81.8
$\sigma=L_d/L_q$	3.61	4.63	5.1	8.13	6.42

low power factor) and a low inductance difference  $\Delta L=L_d-L_q$ . This can be explained by the fact that  $\sigma$  and  $\Delta L$  are not constants but varies with current, and thus  $a_{sc}$ , due to saturation and cross magnetisation [4, 7]. The high current of machine 1, due to the large  $a_{sc}$ , saturates the machine deeply. This lowers specifically the d-axis inductance of the machine, explaining the low  $\sigma$  and the low  $\Delta L$ .

The optimised structure of machine 2 is shown in Fig. 3. The relatively small inner diameter of this machine, and also that of machine 1, is just to obtain more copper area. The ratio of the inner diameter to the outer diameter of machine 2 is 0.52 which is much smaller than the 0.62 of the standard induction machine. This design result was also found and discussed by Vagati [5].

2) *Maximum Efficiency*: Table II shows that the dimensions and the output performances of machines 2 and 3 are almost the same. This can be explained by realising that the copper losses of machine 3 dominate as the greatest part of the total losses so that the efficiency may be taken as

$$\eta \approx \left( 1 + \frac{P_{cu}}{\omega_r T} \right)^{-1} \quad (21)$$

Hence, to maximise the efficiency the  $T/P_{cu}$  has to be maximised which is the same as machine 2 where the torque per 700 W copper losses is maximised.

Machines 1 to 3 of Table II show remarkably high power densities with about the same copper losses and iron losses as that of the standard induction machine. This explains the high efficiencies of these machines. The torque per rotor volume (TRV) is also exceptionally high. For example, machine 2 has a TRV of almost 50 kNm/m<sup>3</sup> which is higher than the range for high performance industrial servos (20-45 kNm/m<sup>3</sup>).

3) *Maximum T/kVA (machine 4)*: By taking the rms supply voltage  $V_s$  as approximately equal to (assuming  $\omega_r$  is constant)

$$V_s \approx \frac{V_q}{\sqrt{2}} \approx K_3 L_d \hat{I}_s \cos(\phi) \quad (22)$$

and dividing (11) by this voltage and the current, the T/kVA after simplifying can be written as

$$\frac{T}{kVA} \approx K_4 \left( 1 - \frac{1}{\sigma} \right) \sin(\phi) \quad (23)$$

where  $\sigma=L_d/L_q$ . Eqn (23) shows that a maximum T/kVA designed RSM will have a large current angle  $\phi$ , a high inductance ratio  $\sigma$  and thus a high power factor, as is clear from Table II, machine 4. With much less current necessary (there is no requirement for high current or high torque) the slot area of this machine will be small (see Fig. 4) and the machine will be out of saturation. Hence,  $L_d$  and thus  $\sigma$  will be high, and the iron losses low. A high  $\sigma$  also enforces a low  $L_q$  which will require the barrier widths and the cutout to be large, as is clear from Table II and Fig. 4.

4) *Constrained Maximum T/kVA (machine 5)*: While machine 4 of Table II has a low output torque, machine 5 is optimised with a constraint on the output torque, namely to be the same as the standard 5.5 kW induction machine. It can be seen that the efficiency of this machine is higher than that of the induction machine, but the power factor is lower. This implies that the same inverter rating will be required.

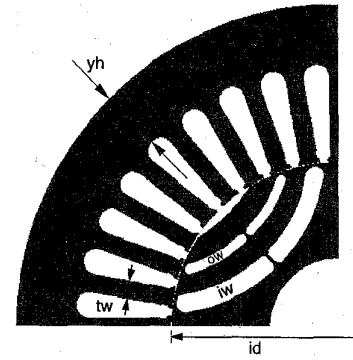


Fig. 3. Stator and rotor structure of the RSM designed for maximum torque (machine 2, Table II).

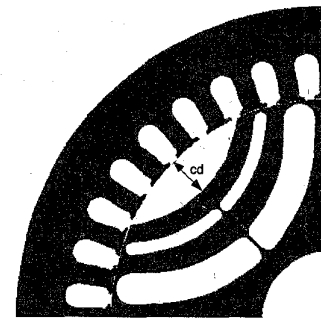


Fig. 4. Stator and rotor structure of the RSM designed for maximum torque/kVA (machine 4, Table II).

## VI. MEASURED RESULTS

Machine 2 of Table II has been build in a standard induction machine frame with the rotor skewed by one stator slot pitch. The machine is controlled by a transputer system and an analog current regulator together with an IGBT inverter. Tests were conducted on the machine to compare the finite element calculations with measurements.

In the finite element calculations the d-axis current  $I_d$  is set constant while the q-axis current  $I_q$  is varied to vary the torque of the machine. The variation of the actual stator current components,  $I_{d1}$  and  $I_{q1}$ , with  $I_q$  is also determined. The calculated results are shown in Fig. 5 where the torque and d-axis current  $I_{d1}$  are plotted against the q-axis current  $I_{q1}$ .

The d-axis current  $I_{d1}$  of Fig. 5 is used in the control system for the desired d-axis current of the RSM-drive. With this at a speed of 1000 r/min, the machine is loaded and the measured shaft torque versus  $I_{q1}$  is determined as shown in Fig. 5. The close agreement between calculated and measured results confirms the remarkably high power density of this machine.

## VII. CONCLUSIONS

From the calculated and measured results the following conclusions are drawn:

(i) It is possible to do a total (stator and rotor) unconstrained or constrained optimum design of the RSM using finite element

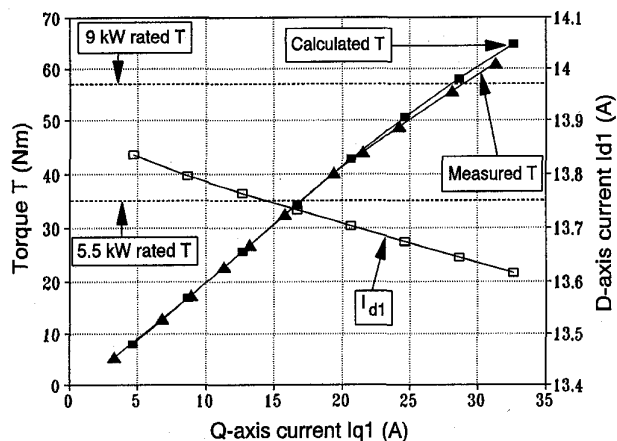


Fig. 5: Calculated and measured results of the 9 kW machine 2.

analysis directly in the optimisation procedure.

(ii) Optimisation algorithms which require that the function's gradient, or first partial derivatives, be computed, can be used with success using the nonlinear finite element field solution to calculate the function value.

(iii) The stator dimensions of the optimum designed RSM, specifically the inner diameter, can differ quite dramatically from that of the standard induction machine. It is thus unfair to compare the performance of this machine with other machines using an induction machine stator.

(iv) The high power density and high efficiency of the RSM, obtained here in the sub 10 kW power range, are clearly the advantages of this machine.

### VIII. ACKNOWLEDGMENT

The authors gratefully acknowledge the contribution of Johan D. Buys and the financial assistance of ESKOM, SPOORNET and the FRD of South Africa.

### REFERENCES

- [1] T.A. Lipo, "Synchronous reluctance machines - a viable alternative for AC drives", *Electr. Mach. Power Syst.*, vol.19, pp. 659-671, 1991.
- [2] A. Vagati, "The synchronous reluctance solution: a new alternative in A.C. drives", *Proc IEEE IECON'94* (Bologna), vol. 1, pp.1-13, 1994.
- [3] L. Xu, X. Xu, T.A. Lipo and D.W. Novotny, "Vector control of a synchronous reluctance motor including saturation and iron loss", *IEEE Trans. Industry Applications.*, vol. 27, no. 5, pp. 977-987, Sept. 1991.
- [4] M.J. Kamper and A.T. Mackay, "Optimum control of the reluctance synchronous machine with a cageless flux barrier rotor", *Trans. S.A. Institute of Electrical Engineers*, vol. 86, no. 2, pp.49-56, June 1995.
- [5] A. Vagati, G. Franceschini, I. Marongiu and G.P. Troglia, "Design criteria of high performance synchronous reluctance motors", *IEEE-IAS annual meeting record*, pp. 66-73, Sept. 1992.
- [6] T. Matsuo and T.A. Lipo, "Rotor design optimization of synchronous reluctance machine", *IEEE Trans. on Energy Conversion*, vol. 9, no. 2, pp. 359-365, June 1994.
- [7] M.J. Kamper and A.F. Volschenk, "Effect of rotor dimensions and cross magnetisation on  $L_d$  and  $L_q$  inductances of reluctance synchronous machine with cageless flux barrier rotor", *IEE Proc.-Electr. Power Appl.*, vol. 141, no. 4, July 1994.
- [8] V.B. Honsinger, "Theory of endwinding leakage reactance", *Trans. AIEE*, vol. 78, no. 3, pp.417-426, 1959.

- [9] M.J. Kamper, *Design criteria of squirrel-cage induction motors*, M.Eng. thesis, Univ. of Stellenbosch, pp. 93-103, 1987.
- [10] P.J. Lawrenson, "Calculation of machine endwinding inductances with special reference to turbogenerators", *Proc. IEE*, vol. 117, no. 6, pp.1129-1134.
- [11] T.J. Flack and A.F. Volschenk, "Computational aspects of time-stepping finite-element analysis using an airgap element", *ICEM*, Sept 1994.
- [12] M.A. Alhamadi and N.A. Demerdash, "Modelling of effects of skewing of rotor mounted permanent magnets on the performance of brushless DC motors", *IEEE Trans. on Energy Conversion*, vol. 6, no. 4, pp. 721-729, 1991.
- [13] S. Williamson, T.J. Flack and A.F. Volschenk, "Representation of skew in time-stepped two-dimensional finite element models of electrical machines", *IEEE-IAS annual record meeting*, pp. 143-148, 1994.
- [14] M.J.D. Powell, "An efficient method for finding the minimum of a function of several variables without calculating derivatives", *Computer Journal*, vol. 7, pp. 155-162, 1964.
- [15] P.E. Gill, W. Murray and M.H. Wright, *Practical optimization*, Academic Press (London), 1981, pp. 117-133 and pp. 335-338.
- [16] D.M. Greig, *Optimisation*, Longman (London), 1980, pp. 49-59.
- [17] W.H. Press, B.P. Flannery, S.A. Teukolsky and W.T. Vetterling, *Numerical recipes*, Cambridge university press, 1986, pp. 294-312.
- [18] R.R. Barton, "Computing forward difference derivatives in engineering optimization", *Eng. Opt.*, vol. 20, pp. 205-224, 1992.



Maarten J. Kamper was born in South Africa in 1959. He received the B.Eng. (1983) and M.Eng.(1987) degrees from the University of Stellenbosch. He was employed by the South African Transport Services and the South African Council for Scientific and Industrial Research. He joined the lecturing staff of the University of Stellenbosch in 1989 as senior lecturer. His main research interests are electrical machines, power electronics and variable speed drives. He is a registered professional engineer in South Africa.



Frederik S. van der Merwe (M'76, SM'79) was born in South Africa in 1939. He received the B.Sc., B.Eng. degrees from the University of Stellenbosch in 1962, the M.Sc.(Eng.) degree from the University of London in 1965 and the Ph.D.(Eng.) degree from the University of Stellenbosch in 1976. His main research interests are electrical machines and variable speed drives. He is a registered professional engineer in South Africa and a Fellow of the South African Institute of Electrical Engineers.



Stephen Williamson was born in Manchester, England in 1948. He attended Imperial College, London, where he gained a BSc(Eng) and a PhD. His principal research interests are the design and analysis of induction machines, for which he has developed both finite-element and algebraic models. Current research is focussed on the modelling of special forms of machine and single phase motors. He is currently Professor of Engineering at the University of Cambridge, a Fellow of the IEE, and of the IEE in London.

### Discussion

**A.J. Urdaneta, C.Candela** (Universidad Simón Bolívar),  
**M. Cerrolaza** (Universidad Central de Venezuela)  
**R. Diaz** (C.V.G. EDELCA) :

The authors are to be commended for an excellent work and a very interesting article devoted to the calculation of the overall optimal design of an electrical machine using detailed, realistic, simulations performed by means of a well known finite-element algorithm.

A similar research, but applied to the optimal design of other types of electrical apparatus is been conducted at Universidad Simón Bolívar. [A] Our comments are mostly directed to the solution methodology, rather than to the specific problem solved in the paper.

In our case, the three layer approach described by Fig.1 was applied, [B] together with a conventional mesh generator and a finite element numerical simulator.

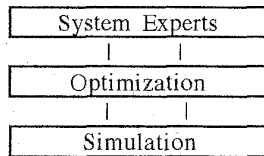


Fig.1. Solution Scheme [B]

The author's comments on the following points are highly appreciated.

**I )** Due to the nonlinear nature of the problem, the optimality of the solution obtained by the proposed algorithm is guaranteed only for the specific operation conditions that were given for the application of the design procedure. For a different point, the optimal solution may change.

Besides, in the design procedure, different factors may play an important role, determining therefore, distinct objective functions which need to be optimized as well. Therefore, in general, from a theoretical point of view, the optimization problem must be set and solved considering different, "relevant" scenario, and not only the "worst" or main case as in the classical min-max approach. [B]

**II )** During the calculation process, the optimization algorithm may require the simulation of non-feasible points, leading to calculation problems in the finite element simulation procedure, and therefore to troubles in the evaluation of the objective function. In our case, this situation was handled by interrupting the problematic simulations and by feeding back a constant, very high value for the objective function being minimized.

**III )** Our limited experience with this approach, when applied to other problems of the electrical engineering field, [B][C][D] reveals a certain advantage of the method of Hooke & Jeeves (based solely upon numerical evaluations of the objective function and the constraints) when compared to other well known optimization techniques such as the algorithms proposed by Powell, Rosenbrock and the Box or Complex method.

Finally, we would like to congratulate the authors for a pioneer application of an optimization algorithm based upon finite element simulation techniques, which opens a broad panorama of new possibilities, and particularly allowing the calculation of an overall optimum design of synchronous machines.

### References

- [A] Diaz, R., "Optimal Design of Electrical Devices Using Finite Element Techniques", Thesis M.Sc. (Spanish) Universidad Simón Bolívar, Caracas, Venezuela, 1.995.  
 [B] Urdaneta, A.J., Chankong, V., "A Multiple Objective Minimax Approach to Controller Settings for Systems Running Under Disturbances", *Invited Paper, Control: Theory and Advanced Technology*, Special Edition on "Multiple Objective Discrete Dynamic Systems: Theory and Applications", MITA PRESS, Tokyo, Japan, December, 1989.  
 [C] Urdaneta, A.J., Bacalao, N., Feijóo, B., Flores, L., Diaz, R., "Tuning of Power System Stabilizers Using Optimization Techniques", *IEEE Trans. on Power Systems*, Vol.6, No.1, February, 1991.  
 [D] Urdaneta, A.J., Nadira, R., Pérez, L.G., "Optimal Coordination of Directional Overcurrent Relays in Interconnected Power Systems", *IEEE Trans. PWRD*, July, 1988, pp. 903-911.

Manuscript received February 28, 1996.

**M.J. Kamper:** The authors welcome the discussion and would like to respond as follows on the three points:

(i) The focus of the paper is on the question about the performance capability of the reluctance synchronous machine. As a *first step* to answer this question using finite element analysis in the design optimisation only single objective functions, such as rated torque per given losses, are considered. The latter is done to characterise the RSM in comparison with other machines, in this case the standard induction machine. But agreed, there are other important factors (determining different objective functions) such as cost and weight of the machine to be considered, then in a multiple objective min-max approach.

(ii) In our design program each machine variable  $x_i$  to be optimised is given minimum and maximum boundary values wherein the variable is allowed to vary. The latter is done to ensure that the minimisation process is within the allowed n-dimensional space. If the minimum or maximum of the function is not in the allowed n-dimensional space, then the program either shifts the boundary values or, if this is not allowed, uses penalty functions to penalise the function value.

(iii) It seems from literature that the Hooke-Jeeves method is time efficient. Li and Rahman [1] makes use of a modified Hooke-Jeeves method (based on the direct search method of Hooke and Jeeves [2]) in the optimum design of the induction

machine. They found that this method is very time efficient compare to other methods. As time efficiency (or number of solutions) is of the utmost importance when using finite element analysis, it would be interesting to compare this method with the Powell and Quasi-Newton methods. The aim of our study was to use (evaluate) well-known gradient and non-gradient methods.

#### References

[1] C. Li and A. Rahman, "Three-phase induction motor

Manuscript received April 1, 1996.

design optimisation using the modified Hooke-Jeeves method", *Electric Machines and Power Systems*, vol. 18, pp. 1-12, 1990.

[2] R. Hooke and T.A. Jeeves, "Direct search solution of numerical and statistical problem", *Journal of ACM*, vol. 8, pp. 212, 1961.